Stiffness of Single-Walled Carbon Nanotubes under Large Strain

T. Ozaki, Y. Iwasa, and T. Mitani

Japan Advanced Institute of Science and Technology, Tatsunokuchi Ishikawa 923-1292, Japan

(Received 21 September 1999)

Large-scale molecular dynamic simulations of the axial deformations in single-walled carbon nanotubes have been performed using an $O(N)$ tight-binding method. Our simulations indicate that under large strain, 0 K stress is remarkably sensitive to helicity, and that a zigzag nanotube and an armchair nanotube are the stiffest, respectively, under elongation and compression regimes. Furthermore, the elastic properties of a graphite sheet have been investigated using a simple harmonic potential and an analytic bond-order potential. The results suggest that the unique elastic properties of carbon nanotubes originate from those of a six-membered ring.

PACS numbers: 61.48.+c

Ever since the discovery of carbon nanotubes (CNT) by Iijima [1], enormous fundamental and applied research has been in progress [2]. Among them, several experiments [3] and theoretical predictions [4–7] have revealed the remarkable mechanical properties of CNTs. These mechanical properties may be characterized by the following three features. First, the mechanical properties are highly anisotropic. Second, the Young's modulus ($\simeq$ 1 TPa) is comparable to that of a diamond. Third, when a CNT that has been bent is released from the strain, it returns to its original form without causing any direct fracture like most materials. These prominent mechanical properties lend themselves to a wide variety of potential applications.

So far, several groups have theoretically predicted that mechanical properties under small strain such as Young's modulus are insensitive to helicity [4,5]. Such helicity independent mechanical properties contrast sharply with those electronic properties that are crucially controlled by helicity. However, the effect of helicity, in other words, the arrangement of six-membered rings, may affect the mechanical properties under such conditions as large strain.

In this Letter, the researchers aim to clarify the relation between stress and helicity of single-walled carbon nanotubes (SWNT) under large strain by means of atomistic lattice mechanics. First, large-scale molecular dynamic (MD) simulations of axial elongation and compression of SWNTs are performed at 0 and 300 K using an $O(N)$ tight-binding (TB) method. Second, the strain energy values of SWNTs are compared with those of a graphite sheet under large strain. Third, the strain energy values of a graphite sheet are analyzed by two model potentials, a simple harmonic potential and an analytic bond-order potential (BOP).

The recent progress of $O(N)$ methods in TB electronic structure calculations [8] allows us to perform direct MD simulations based on a quantum mechanical TB Hamiltonian [9] for large systems that include thousands of atoms. To investigate the effects of helicity, we performed MD simulations of elongation and compression for a series of $(10, 10)$, $(12, 8)$, $(14, 5)$, $(16, 2)$, and $(17, 0)$ SWNTs, which have a nearly equal radius ($\simeq$ 6.7 Å) and a length of 140 Å, at $T = 0$ and 300 K using the $O(N)$ TB method [10]. In these simulations, the end atoms were shifted along the axis by small steps, and the whole tube was optimized by the conjugate-gradient method, while keeping the ends constrained after, in the 300 K simulations, constant temperature MD simulations were performed at 300 K for 0.1 ps using the Nose-Hoover algorithm [11] with the constraint.

Remarkable temperature effects were observed in the strain and shape of buckling under compression as shown in Fig. 1. At 0 and 300 K the five SWNTs buckle at about 19% and 10% of the compressed strain, respectively. In the $(10, 10)$ nanotube at 80% of the initial length, the mean wave lengths of the ripple buckling at 0 and 300 K are about 4.8 and 13 Å, respectively. The long range buckling at 300 K makes the helical dependence of the stress indistinct under large strain, since the local strain of each atom in the SWNT is released at an early stage of compression compared with that of compression at 0 K. Although the temperature dependence of the buckling morphology is very intriguing as a bifurcation phenomenon, we concentrated on the relation between stress and helicity at 0 K before the buckling occurred.

In Fig. 2(a) the strain energy values per unit length of the armchair $(10, 10)$ and zigzag $(17, 0)$ tubes under elongation and compression at 0 K are shown as a function of

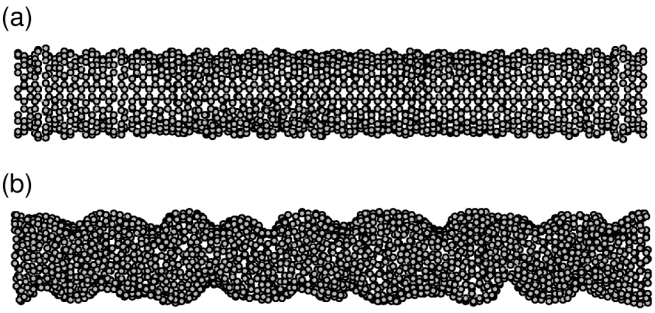

FIG. 1. Buckling of $(10, 10)$ nanotubes, which include 2280 carbon atoms, under axial compression at (a) 0 and (b) 300 K obtained by $O(N)$ TBMD simulations. These snapshots are at 80% of the initial length (140 Å).

 0031-9007/00/84(8)/1712(4)$15.00

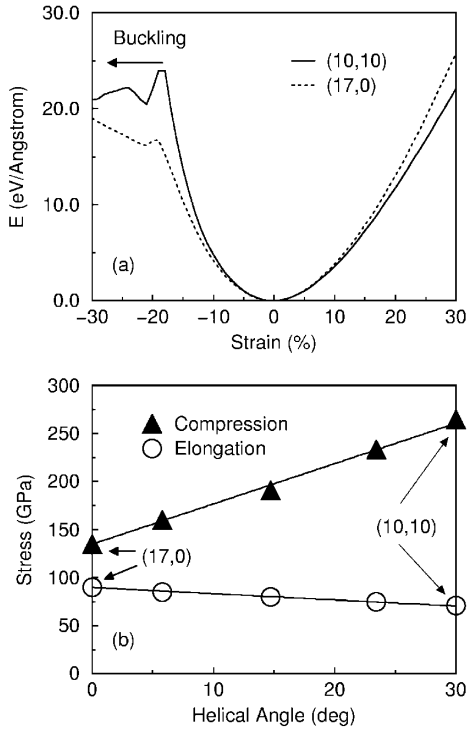

FIG. 2. (a) Strain energy values of the armchair $(10, 10)$ and zigzag $(17, 0)$ tubes as a function of the axial strain at 0 K. (b) Axial stresses of SWNTs which have a nearly equal radius ($\simeq$ 6.7 Å) at 15% of the axial compression and elongation at 0 K.

the strain. The Young's moduli of the zigzag and armchair tubes are 988 and 973 GPa, respectively, where they were calculated according to the definition of Lu [5]. The values of the Young's moduli are almost identical with his results, and the insensitivity for helicity is also consistent with the predictions made by other groups [4]. On the other hand, the strain energy under large strain conditions shows significant sensitivity to helicity. Figure 2(b) shows axial stresses at 15% of elongation and compression at 0 K, quantities which are calculated numerically as slopes of the strain energy values, as a function of the helical angle. Although the stresses for both elongation and compression depend almost linearly on the helical angle, the slopes are opposite to each other. The stiffest SWNT for elongation is the $(17, 0)$ zigzag tube, while that for compression is the $(10, 10)$ armchair tube. In particular, the stress of the armchair $(10, 10)$ tube is about double that of the $(17, 0)$ zigzag tube for compression. So far it has been reported that the onset of plastic deformation under elongation depends on helicity [6]. This is the first demonstration of helicity dependence on stress (stiffness), as well as its turning over between the elongation and compression processes. Figure 2(a) indicates that the remarkable elastic properties under large strain are caused by nonparabolic strain energy.

We next investigated the origin of the nonlinear elastic properties of the SWNTs under large strain in terms of atomistic lattice mechanics. To separate the effects of the tube structure from those of a graphite structure on the nonparabolic strain energy, the strain energy values of the $(10, 10)$ armchair and $(17, 0)$ zigzag tubes were compared with those of unfolded graphite sheets calculated with the TB model. Figure 3(a) shows the strain energy values of a graphite sheet per unit cell and per unit length under two kinds of strain: A strain and Z strain correspond to the axial strains for armchair and zigzag tubes, respectively. The unit cell includes four carbon atoms, and the norms of the orthogonalized unit vectors $\mathbf{a}$ and $\mathbf{b}$ are $|\mathbf{a}| = 2r_2 \sin\theta_1$ and $|\mathbf{b}| = 2r_1 - 2r_2 \cos\theta_1$, respectively [Fig. 3(a), inset]. These structural optimizations were performed with the atoms maintained in the two-dimensional sheet, where the changes in the length of the cell vector perpendicular to the strained axis were -2.6% and -2.4% at the A and Z strains of 10%, and 3.8% and 3.7% at those of -10%, respectively. The A strain energy per unit cell is larger than that of the Z strain under both elongation and compression, implying that the six-membered ring behaves differently depending on the direction of stress.

The A- and Z-strain energy values in Fig. 3(b) were obtained by simply multiplying the A- and Z-strain values in Fig. 3(a) by 10 and 17, respectively, which correspond to the A- and Z-strain energy values per two kinds of supercells. The sets of the cell vectors of the two supercells are $(\mathbf{a}, 10\mathbf{b})$ and $(17\mathbf{a}, \mathbf{b})$, which correspond to the developments of the $(10, 10)$ armchair and $(17, 0)$ zigzag

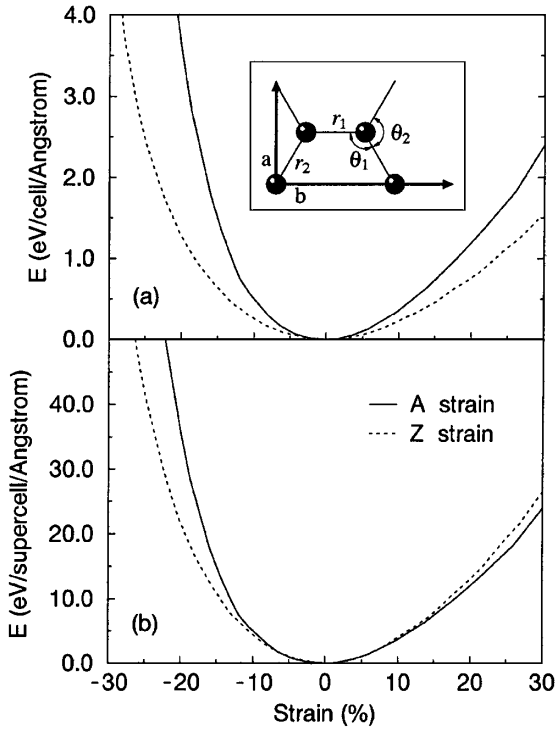

FIG. 3. (a) Strain energy values of the graphite sheet per unit cell and per unit length for the A strain and Z strain. (b) Strain energy values of the graphite sheet per supercells $(\mathbf{a}, 10\mathbf{b})$ and $(17\mathbf{a}, \mathbf{b})$ and per unit length for A strain and Z strain, respectively.

tubes, respectively. The strain energy values of the two supercells cross each other at the origin, while the strain energy values per unit cell are positioned tangentially to each other at the origin as shown in Fig. 3(a). The energy crossing is caused by the competition between the number of six-membered rings in the supercells and the directional dependence of a six-membered ring in strain energy, and by the difference between nonparabolicity for the A and Z strains in strain energy per unit cell. A comparison between Fig. 2(a) and Fig. 3(b) led us to the conclusion that the crossing of the two strain energy values at the origin in Fig. 2(a) is due more to the nonlinear elastic properties of the graphite sheet than the effects of the tube structure. Hence, the nonlinear elastic properties of SWNTs can be broken down into two contributions: the directional dependence of the nonlinear elastic properties of a six-membered ring, and the number of rings on the circumference of the SWNT.

Next, we considered a simple harmonic model for the graphite sheet in order to relate the elastic properties of the sheet with the strain of the bond lengths and bond angles in a six-membered ring. In addition, the strain energy values of the harmonic model were compared with those of BOP [12] within a second moment approximation to reveal the quantum mechanical origin of the nonparabolic strain energy. Assuming that the harmonic model includes bond-stretching (BS) and angle-bending (AB) energy, we can express the strain energy E_{h} of the graphite sheet per unit cell [see Fig. 3(a), inset] as follows:

$$E_{\mathrm{h}} = k_r(r_1 - r_0)^2 + 2k_r(r_2 - r_0)^2 + 4k_\theta(\theta_1 - \theta_0)^2 + 2k_\theta(\theta_2 - \theta_0)^2, \qquad (1)$$

where r_0 and θ_0 are the optimum values, and k_r and k_θ are the spring constants. We analyzed the model potential in two extreme situations: $k_\theta \ll k_r$ and $k_r \ll k_\theta$.

When $k_\theta \ll k_r$, which means that the bond lengths are fixed, only AB energy contributes to the strain energy Eq. (1). Assuming that atoms are confined in a plane, bond angle θ_1 behaves as a spring which has 4 times the strength of bond angle θ_2 for any strain, since the sum of the interior angles of the six-membered ring is a constant. In Fig. 4(a) the strain energy values in Eq. (1) for $k_\theta \ll k_r$ per unit length are shown as a function of the percentages of the A and Z strains. Both the A- and Z-strain energy values increase remarkably under elongation, notably the maximum elongating strain on A strain, which is $[(2 - \sqrt{3})/\sqrt{3}] \times 100 \simeq 15.5\%$. When $k_r \ll k_\theta$, the bond angle is fixed. In the case of A strain, since the bond length r_1 is constant and the strain energy is determined by only the BS energy on bond 2, the strain energy per unit length for A strain can be expressed as $(2/\sqrt{3})k_r r_0 S_A^2$ with $S_A = (a - a_0)/a_0$. For Z strain, on the other hand, the BS energy values of both bonds 1 and 2 contribute to the strain energy. The strain energy per unit length is given as the solution of a simple extremum problem under a constraint ($|\mathbf{b}| = 2r_1 + r_2$) as $\frac{2}{3}k_r r_0 S_Z^2$ with $S_Z = (b - b_0)/b_0$. Thus, we see that both the strain energy values completely obey Hooke's law under both the A and Z strains with the constraint $k_r \ll k_\theta$ [Fig. 4(c)], indicating that the strain energy of the graphite sheet in the simple harmonic model does not reproduce the nonparabolic behavior seen in Fig. 3(a).

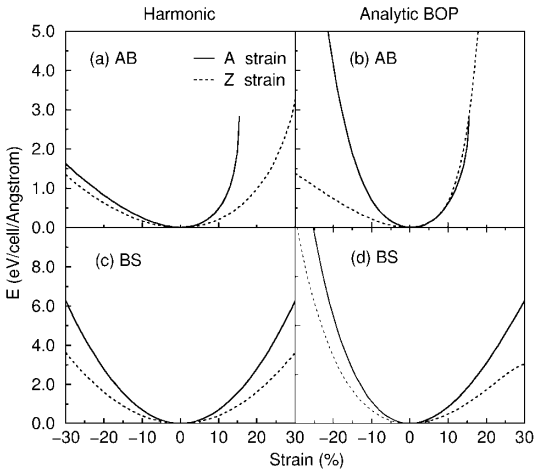

FIG. 4. Strain energy values of a graphitic sheet for the A and Z strains by two model potentials: a harmonic potential and an analytic bond-order potential (BOP). (a), (b), (c), and (d) show the harmonic potential and the analytic BOP in fixing the bond lengths and the bond angles, respectively.

Moreover, the strain energy of a graphite sheet is computed by the analytic BOP [12] within a second moment approximation. The analytic BOP gives an explicit expression, as a function of the bond length and bond angle, of the cohesive energy in the TB model. In the TB model [9], the strain energy E_{BOP} of a graphite sheet is defined as the difference between the sum of two energy values, the bond energy E_{bond} and the repulsive energy E_{rep}, and the nonstrain energy E_0. The bond energy per unit cell [Fig. 3(a), inset] is given by

$$E_{\mathrm{bond}} = -4h_{\sigma_1}\Theta_{\sigma_1} - 4h_{\pi_1}\Theta_{\pi_1} - 8h_{\sigma_2}\Theta_{\sigma_2} - 8h_{\pi_2}\Theta_{\pi_2}, \qquad (2)$$

where each term corresponds to the σ and π bond energy values on bonds 1 and 2, respectively. h_σ and h_π are σ and π hopping integrals, respectively. Within the second moment approximation [12], the bond orders Θ are given as explicit functions of the bond lengths and bond angles for the nearest neighbor atoms as follows:

$$\Theta_{\sigma_1} = \frac{h_{\sigma_1}}{\sqrt{h_{\sigma_1}^2 + 2g_1^2 h_{\sigma_2}^2}}, \qquad (3)$$

$$\Theta_{\pi_1} = \frac{h_{\pi_1}}{\sqrt{h_{\pi_1}^2 + 2h_{\pi_2}^2}}, \qquad (4)$$

$$\Theta_{\sigma_2} = \frac{h_{\sigma_2}}{\sqrt{h_{\sigma_2}^2 + g_1^2 h_{\sigma_1}^2 + g_2^2 h_{\sigma_2}^2}}, \quad (5)$$

$$\Theta_{\pi_2} = \frac{h_{\pi_2}}{\sqrt{h_{\pi_1}^2 + 2h_{\pi_2}^2}}, \quad (6)$$

where g is an angular function on σ bond [12]. The expression of the bond energy clearly shows that the bond angles are related to the bond energy through the σ bond orders. The strain energy given by the analytic BOP is compared with that of the harmonic model for two extreme situations: fixed bond lengths and bond angles in order to decompose the nonparabolic strain energy of the graphite sheet for the A and Z strains into contributions of the bond length and bond angle.

When the bond lengths are fixed, since the π bond energy is invariant for the A and Z strains, the bond energy is given by

$$E_{\text{bond}(r=r_0)} = -4h_{\sigma_0}\left(\frac{1}{\sqrt{1 + 2g_1^2}} + \frac{2}{\sqrt{1 + g_1^2 + g_2^2}}\right), \quad (7)$$

where $h_{\sigma_0} = 12.71$ eV. Figure 4(b) shows the strain energy values for the A and Z strains by the analytic BOP in fixing the bond lengths. From a comparison between Figs. 4(a) and 4(b) we see that the strain energy of the analytic BOP increases significantly compared with that of the harmonic model in the compression of the A strain as well as in the elongation of the Z strain. The increase of this energy can be attributed to the repulsive energy occurring between the second nearest neighboring atoms, since the nonparabolic behavior of Eq. (7) for the A and Z strains is very similar to that of the harmonic model, and the repulsive energy occurring between the nearest neighboring atoms is invariant. When the bond angles are fixed, on the other hand, the strain energy for the A and Z strains is determined numerically under the constraints of $|\mathbf{a}| = \sqrt{3}\, r_2$ and $|\mathbf{b}| = 2r_1 + r_2$, respectively. Figure 4(d) shows the strain energy for the A and Z strains. The strain energy values are significantly nonparabolic and quite similar to those in Fig. 3(a) compared with Fig. 4(c).

The separation of the bond-stretching and angle-bending models provides a clear explanation for the origin of the nonparabolic strain energy observed in the graphite sheet. That is, the nonparabolic behavior of the strain energy shown in Fig. 3(a) results predominantly from that of bond stretching rather than that of angle bending, and the crossing of the two strain energy values for the A and Z strains comes from the magnitude of the repulsive energy between the second neighboring atoms under compression, which causes the considerably helicity dependence of the stress of SWNT under large strain at 0 K.

In summary, our $O(N)$ TB simulations indicate that the buckling shape of SWNTs depend greatly on the temperature of the system, and that stress under large strain at 0 K is very sensitive to helicity. Under both elongation and compression the stresses of SWNTs with a nearly equal radius depends almost linearly on a helical angle with the opposite slopes, and the stiffest SWNTs are a zigzag and armchair tube, respectively. A comparison between SWNTs and a graphite sheet in strain energy reveals that helicity dependence of the stress is caused by the graphite structure rather than the tube structure. Moreover, we investigated the strain energy of a graphite sheet with a harmonic model and an analytic BOP, which gives an explanation for the nonparabolic strain energy values of the A and Z strains. Thus, we conclude that the mechanical properties of SWNTs under large strain at 0 K significantly reflect the network structure.

This work has been supported by the JSPS "Future Program," and also by the Grant-In-Aid for Scientific Research on the Priority Area "Fullerenes and Nanotubes."

[1] S. Iijima, Nature (London) **354**, 56 (1991).
[2] H. Dai *et al.,* Nature (London) **384**, 147 (1996); C. Dillon *et al.,* Nature (London) **386**, 377 (1997); J. W. G. Wildoer *et al.,* Nature (London) **391**, 59 (1998); T. W. Odom *et al.,* Nature (London) **391**, 62 (1998).
[3] S. Iijima *et al.,* J. Chem. Phys. **104**, 2089 (1996); M. R. Falvo *et al.,* Nature (London) **389**, 582 (1997); Jean-Paul Salvetat *et al.,* Phys. Rev. Lett. **82**, 944 (1999).
[4] G. Adams *et al.,* Science **256**, 1792 (1992); D. Robertson *et al.,* Phys. Rev. B **45**, 12 592 (1992); A. Lucas *et al.,* J. Phys. Chem. Solids **54**, 587 (1993); B. I. Yakobson *et al.,* Phys. Rev. Lett. **76**, 2511 (1996).
[5] J. P. Lu, Phys. Rev. Lett. **79**, 1297 (1997).
[6] P. Zhang, P. E. Lammert, and V. H. Crespi, Phys. Rev. Lett. **81**, 5346 (1998).
[7] D. Srivastava, M. Menon, and K. Cho, Phys. Rev. Lett. **83**, 2973 (1999).
[8] T. Ozaki, Phys. Rev. B **59**, 16061 (1999); T. Ozaki, M. Aoki, and D. G. Pettifor, Phys. Rev. B (to be published).
[9] C. H. Xu, C. Z. Wang, C. T. Chan, and K. M. Ho, J. Phys. Condens. Matter **4**, 6047 (1992).
[10] The $O(N)$ method was applied with a three hop logically truncated cluster, 12 recursion levels, a square root terminator, and $k_B T = 0.1$ eV reproducing cohesive energies of a graphite sheet and SWNTs within errors of 1% compared with the k-space results (see Ref. [8]).
[11] S. Nose, Mol. Phys. **52**, 255 (1984); W. Hoover, Phys. Rev. A **31**, 1695 (1985).
[12] D. G. Pettifor and I. I. Oleinik, Phys. Rev. B **59**, 8487 (1999); **59**, 8500 (1999), and references therein.